Film Formations of Aggregates Due to Lateral Capillary Forces

Mark Doran[1]*, Paul Dastoor[2], Murray Sciffer[2] and Roberto Moreno-Atanasio[1]

[1] School of Engineering,
The University of Newcastle, Callaghan
New South Wales 2308, Australia
*e-mail: mark.doran@uon.edu.au

[2] School of Mathematics and Physical Sciences
The University of Newcastle, Callaghan
New South Wales 2308, Australia

Key words: DEM, lateral capillary forces, self-organisation, film formation binary dispersed.

Abstract. The lateral capillary force is of significant importance in liquid film coating processes [1]. This force, for particles much smaller than the capillary length, decays with the inverse of the separation distance between particles centres and is, thus, considered a long-range force [2]. In this paper, we study the role of this long-range force on the final structure of a film containing partially submerged nanoparticles.

We have used computer simulations based on Discrete Element Method (DEM) to investigate film formation of mono and binary disperse particle systems. The particle radii were 80 nm, 100 nm, and 120 nm with combinations of these particle sizes for the binary disperse system. To determine the nearest neighbours for the calculation of the lateral capillary force a Delaunay Triangulation method was used. The surface coverage of the partially submerged particles was 0.05, which coincides with a parallel experimental research. The forces included in the model are the lateral and vertical capillary forces, Brownian motion, contact forces, van der Waals attraction, fluid drag and hydrodynamic resistance. The structure of the aggregates formed was compared using three parameters, the isotropic ordering factor, non-dimensional boundary length and the pair (radial) correlation function.

The simulation results show that particles self-organise into isotropic aggregates due to lateral capillary forces. Particle size was shown to have little effect on final aggregate structures. Binary disperse systems were shown to have less ordered structures when compared to monodisperse systems as suggested by the decrease in peak sharpness of the pair correlation function. Increasing the particle size gap resulted in less ordering in the binary systems.

1 Introduction

Lateral capillary forces play an important role in the self-assembly of partially immersed particles. By being able to control the lateral capillary forces it is possible to form complex structures such as hexagonal packing [1,3]. Bowden et al [4] used lateral capillary forces between hexagonal particles floating on liquid surfaces to form a range of structures depending on the wetting of the hexagon faces. Similarly, the aim of this work is to harness the strength of lateral capillary forces that exist between organic nanoparticles to optimise the film structure of organic photovoltaic layers, which can affect the device efficiency [5–7].

Lateral capillary forces occur between particles partially immersed in a liquid. Lateral capillary forces are due to deformation of the liquid surface meniscus and has been studied both experimentally and theoretically [2,8–14]. Bragg and Nye [15] experimentally used capillary interaction forces to create two-dimensional arrays of bubbles floating on the surface of a soap solution. The crystal structures were used to compare the defects in the bubble arrays to defects in metallic lattices. The first attempt to quantitatively describe the capillary force

between bubbles floating on a liquid surface was by Nicholson [16], which was valid for bubbles less than 3 mm where a linearised solution to the Young-Laplace equation is valid.

The capillary force has been studied for many different geometries, such as floating horizontal cylinders [17], flat plates [18,19], vertical cylinders [19], spheres [19], particles and walls [8,14,19] and cubes [20]. The capillary force is different for each of these due to the solution of the Young-Laplace equation being geometry dependent. A detailed review of capillary forces can be found in Ref [21].

The Lattice Boltzmann numerical method has also been used to study lateral capillary forces [22,23], as well as several discrete element method (DEM) models [1,3,24,25]. Maenosono et al. [24] showed that over time particles, with diameters of 55 nm and 155 nm, form a cluster of hexagonal packing. They also found the presence of point defects, which occur is consistent their experimental research [26]. Nishikawa et al. [25] showed the formation of chain like structures at lower particle coverage, while at high coverage domains of hexagonal close packing were formed.

Fujita et al. [3] include other interparticle forces in their simulations. They showed that during evaporation the magnitude of the capillary, Brownian, electrostatic and van der Waals change and hence the concluded that all these forces played an important role on the self-ordering of particles. Depending on the magnitude of these forces three types of structures were formed; isotropic crystals, non-isotropic aggregates and isotropic arrangements. Due to the computational time required to determine the lateral capillary force Uzi, Ostrovski & Levy [1] developed a new model to calculate the capillary force which did not require the calculation of the liquid surface deformation directly. They found that particle size did not affect the final structures obtained.

This paper uses a DEM model to investigate the lateral capillary force on film formation. The previously mentioned DEM models [1,3,24] simulate similar systems with monodisperse particles. It is our intention to investigate the influence of particle size on the film formation due to lateral capillary forces. The simulations consists of binary dispersed particles systems and compare these to monodisperse systems. An important difference with previous studies in the literature is the use of binary particle distributions. These type of studies have never been carried out in the past.

2 Methodology

2.1 Discrete Element Method

DEM is a numerical computational technique that uses Newton's second law of motion to describe the motion of individual particles. This method was first developed by Cundall and Strack to study the motion of rocks [27]. The motion equation used in our computational model involves capillary forces, Brownian motion, contact forces, short range attractive forces, drag and hydrodynamic resistance. The motion equation is given by

$$m\frac{d\vec{r}^2}{dt^2} = \vec{F}_{cap} + \vec{F}_{brw} + \vec{F}_{cont} + \vec{F}_{vdw} + \vec{F}_{drag} + \vec{F}_{hyd} \quad (1)$$

where m is the mass, $\vec{r}$ is the displacement, t is time and $\vec{F}$ is the external force. The subscripts cap, brw, cont, vdw, drag and hyd refer to capillary forces, Brownian motion, contact forces, van der Waals interactions, fluid drag and hydrodynamic resistance respectively.

The capillary force is decomposed into vertical and lateral capillary directions. The vertical capillary force is given by Equation 2 [28].

$$\vec{F}_{vcap} = -2\pi\gamma R\sin(\theta)\sin(\theta+\varphi) \quad (2)$$

where γ is the surface tension, R is the particle radius, θ is the contact angle and ψ is the filling wetting angle.

The lateral capillary force is given by Equation 3 [29].

$$\vec{F}_{lcap} = 2\pi\gamma Q_i Q_j q K_1(qL) \quad (3)$$

where Q_i is the capillary charge $Q_i = r_i \sin(\varphi_i)$, q is the inverse of the capillary length $q=\sqrt{\frac{\rho g}{\gamma}}$, K_1 is the modified Bessel function of the second kind and L is the lateral distance between particle centres. An asymptotic solution valid when qL>>1 can be used to avoid computation of the modified Bessel function which reduces to Equation 3 to Equation 4 [14].

$$\vec{F}_{lcap} = \frac{2\pi\gamma Q_i Q_j q}{L} \quad (4)$$

The Brownian motion is given by a normal distribution with a mean of 0 and a standard deviation given by Equation 5 [30].

$$\sigma_{brw} = \sqrt{\frac{12\pi k_B T \mu R}{\Delta t}} \quad (5)$$

where k_B is the Boltzmann constant, T is temperature, μ is the liquid viscosity and Δt is the time step.

The contact is modelled by a linear spring dashpot, given by Equation 6 [27].

$$\vec{F}_{cont} = -k_p \delta_{n,} - 2\beta \vec{v}_n \sqrt{m_{ij}\, k_p} \quad (6)$$

where k_p is the spring coefficient, δ_n is the normal overlap, β is the damping coefficient and $\vec{v}_n$ is the normal velocity.

The van der Waals force is given by Equation 7 [31].

$$\vec{F}_{vdw} = \frac{AR_{ij}}{6d^2} \quad (7)$$

where A is the Hamaker constant, R_{ij} is the reduced radii and d is the separation distance between particle surfaces.

The drag force is modelled with stokes drag in Equation 8.

$$\vec{F}_{drag} = -6\pi\mu R\vec{v} \quad (8)$$

The hydrodynamic resistance is given by Equation 9 [32].

$$\vec{F}_{hyd} = -6\pi\mu \frac{R_{ij}^2}{d} \overrightarrow{v_n} \quad (9)$$

2.2 Screening of the lateral capillary force

The lateral capillary force decays with the inverse of the separation distance between particle centres as given by Equation 4 and can be dominant up to many particle radii as it is a long range force. This aspect makes the calculation of the force numerically expensive due to a large neighbour search range. Further complications occur due to the nature of the lateral capillary force. For other long range forces such as the electrical double layer, the total force on any given particle can be approximated using an Ewald summation [33].

The lateral capillary force occurs only between particles that are within the line of sight of each other and so techniques to scan and calculate other long range forces aren't able to be used. Several authors have studied different screening methods [1,3,24,25,34]. These screening methods attempt to scale the capillary force by a ratio, which is dependent on the fraction of neighbouring particles that are within direct line of sight. Then, the nearest neighbours are selected by a cut-off distance with a Vertlet list constructed.

To determine the nearest particles for the lateral capillary force a Delaunay triangulation of particles at the liquid surface was computed. The neighbours are formed from the Delaunay triangulation and the particles are screened using the screening methods in [1].

2.3 Characterisation of the particle aggregates

To quantify the structures that the particles form, three parameters have been used. The isotropic ordering factor (IOF), non-dimensional boundary length (NBL) and the pair (radial) correlation function. The IOF is the ratio of equilateral triangles to the total number of triangles from the constructed Delaunay triangulation. This parameter provides information about the isotropy of the system. The NBL is the ratio of the boundary length of the aggregate compared to the boundary length of a hexagonal packed structure and can be calculated by Equation 10 [3].

$$NBL = \frac{1}{6n}\sum_{k=0}^{6}(6-k)N(k) \tag{10}$$

where n is the number of particles, k is the coordinate number and N(k) is the number of particles with a coordinate number of k.

The IOF is close to 0 for a randomly distributed particle clusters and increases as the clusters become more hexagonally close packed (HCP), with a value of 1 for HCP. The NBL is equal to 1 when the system is randomly dispersed with no particle-particle contacts, and as the particles aggregate the value of the NBL drops reaching 0 when the system is HCP [3].

The pair correlation function g(r), is developed from creating a histogram with particle neighbours separation distance and normalised by Equation 11 [35].

$$g(r) = \frac{1}{N}\sum_{i=1}^{N}\frac{A_0 n_i(r)}{\pi(\delta r^2 + 2r\delta r)} \tag{11}$$

where N is the number of particles, A_0 is the average area per particle, $n_i(r)$ is the number of particles in the interval [r, r+δr]. The pair correlation function can be used to determine the degree of ordering for particle domains [35].

2.4 Simulation Parameters

The particles were initially randomly distributed with a surface coverage of 0.05 (2-D packing). The particle radii were 80 nm, 100 nm and 120 nm, with binary dispersed systems consisting of a combination of these particle sizes. Table 1 lists the simulation parameters.

Table 1: Simulation Parameters.

Parameter	Value	Unit
Number of particles	2000	
Temperature	25	°C
Particle density	1250	kg/m^3
Hamaker constant	1×10^{-20}	J
Spring coefficient	1.0	N/m
Restitution coefficient	0.5	
Time step	1×10^{-10}	s
Liquid density	1000	kg/m^3
Liquid viscosity	1.0	mPa s

3 Results

Figure 1 shows the time evolution of the IOF and NBL for the monodisperse systems with radii of 80 nm, 100 nm and 120 nm. The IOF and NBL start at 0 and 1, respectively, as the particles are randomly dispersed with no contacts. During the first micro second of simulations, the change in the IOF and NBL were very fast with the IOF decreasing and the NBL increasing as time progressed. This clearly suggests that the particles were self-organising due to the lateral capillary force. After this sharp initial change in the IOF and NBL, the rate slows until

the particles are self-organised into one or more large aggregates. The final structure was a crystalline lattice as the final IOF was high while the final NBL was low as suggested by [3]. The final values of IOF and NBL are similar for each particle size suggesting that the particle size has little influence on the self-organisation process, which was also shown by [1]. Further the final value of IOF for all three cases is close to 1, which indicates the crystal shows good isotropic ordering. The difference in time reaching an equilibrium state was due to a larger capillary force between larger particles.

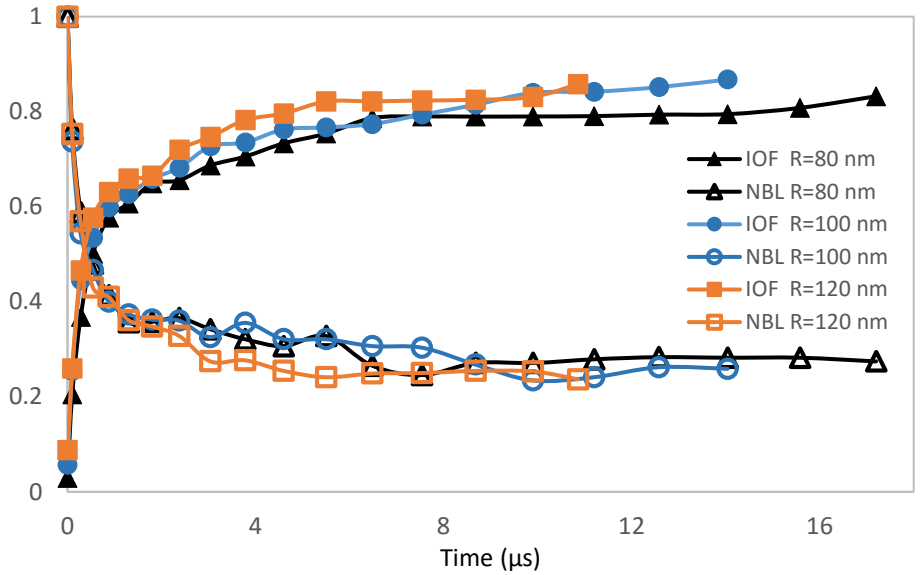

Figure 1: IOF and NBL for monodisperse systems with particle radii of 80, 100 and 120 nm.

The IOF and NBL for the binary particle distribution with particle radii of 80 nm and 100 nm is shown in Figure 2. The trends of the binary particle systems are consistent with the monodisperse systems (Figure 1). There was however little difference between the IOF and NBL of the three binary dispersed systems, despite a visually observable difference in crystalline structure. Therefore, the results for the other three cases have been omitted.

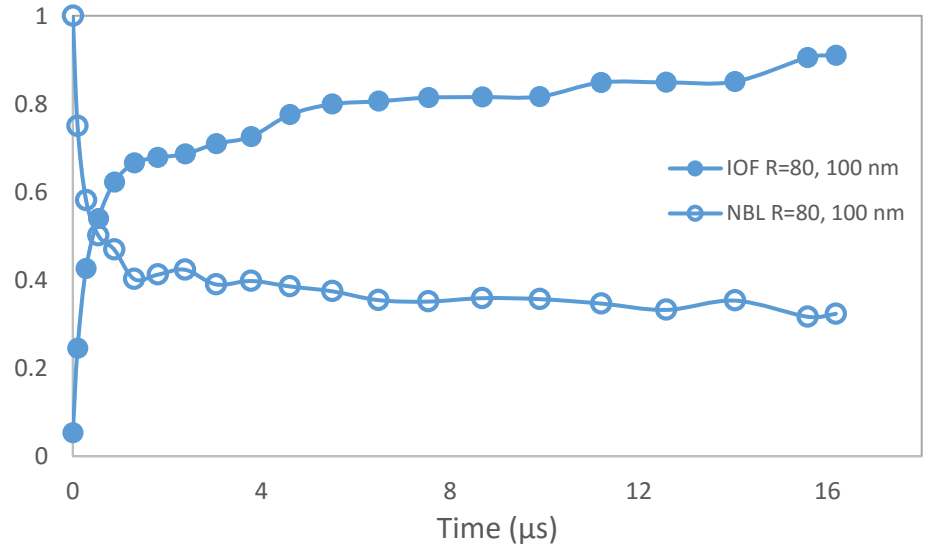

Figure 2: IOF and NBL for binary disperse system with particle radii of 80 and 100 nm.

In order to be able to compare the binary with the monodispersed systems the pair correlation function was used. The pair correlation function of the final structure for the 100 nm particle radii simulation is plotted in Figure 3. The distance is normalised by the particle diameter. The sharp peak at g(r) 1 signifies the particles nearest neighbours. The two peaks between 1.5 and 2 are consistent with a HCP structure, similar to the peaks between 2.5 and 3. The sharpness of these peaks show that the structure has some degree of ordering, consistent with a value of IOF close to 1. The pair correlation for the monodisperse systems with 80 nm and 100 nm particle radii were very similar and omitted due to no observable differences.

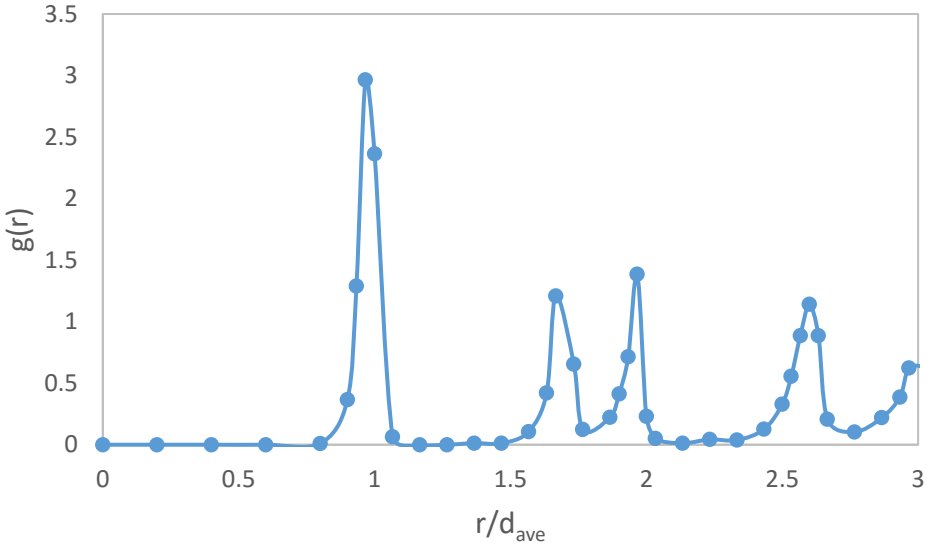

Figure 3: Pair correlation function for monodisperse system with particle radii of 100 nm.

The pair correlation functions plotted in Figure 4a-c are binary systems with particle radii 80-100 nm, 100-120 nm and 80-120 nm respectively, the particle separation distance was normalised by the average radius of particles. The systems with 80-100 nm and 100-120 nm particle radii have the same particle distribution gap of 20 nm. Their pair correlation functions were also similar, further showing that particle size had little effect on the final structures. For Figure 4a-c g(r) had 3 distinct peaks at around a dimensionless distance of 1. However, the monodisperse systems only shown 1 peak. The first of these peaks represent neighbours of the two smaller particle sizes, the middle between the small and large particle and the third between two of the larger particles.

The subsequence dual peaks observed in Figure 3 (monodisperse system) are not present in Figure 4a-c, which signifies a more ordered structure for the monodisperse systems. Figure 4c shows the results for the 80-120 nm binary system, which has a larger particle size distribution of 40 nm. The lack of peaks after the multiple peak around 1 when compared to Figure 4a-b indicates that the difference in particle sizes in binary systems impact the final ordering. Therefore, a narrower size distribution or monodisperse system produces a more ordered structure.

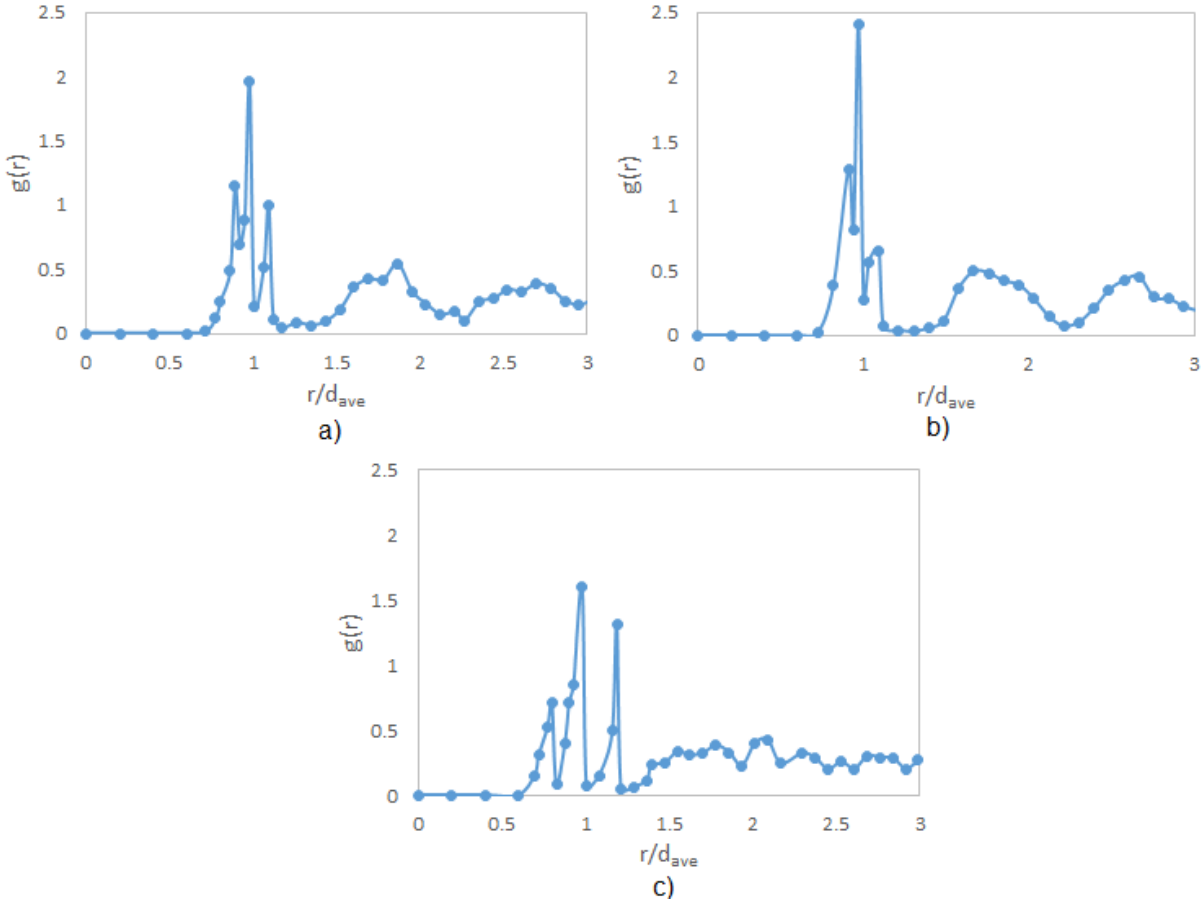

Figure 4: Pair correlation functions for the binary disperse system; a) particle radii of 80 and 100 nm, b) particle radii of 100 and 120 nm and c) particle radii of 80 and 120 nm.

4 Conclusion

The influence of particle size and particle distribution on the self-organisation of partially immersed nanoparticles in a thin liquid film due to lateral capillary forces was investigated using DEM simulations. The particles were found to form isotropic crystal aggregates, with domains of hexagonal packing. The size of particles in the mono and binary dispersed systems was shown to have little effect on the final crystal structure. The binary dispersed systems were found to have less ordered structures when compared to the monodisperse systems. Increasing the particle distribution gap in the binary dispersed system resulted in a less ordered crystalline structure.

5 References

[1] Uzi, A. Ostrovski, Y. and Levy, A. Modeling and simulation of particles in gas-liquid interface. *Adv. Powder Technol.* (2016) **27:** 112–123.

[2] Velev, O.D. Denkov, N.D. Paunov, V.N. Kralchevsky, P.A. and Nagayama, K. Direct Measurement of Lateral Capillary Forces. *Langmuir* (1993) **9:** 3702–3709.

[3] Fujita, M. Nishikawa, H. Okubo, T. and Yamaguchi, Y. Multiscale Simulation of Two-Dimensional Self-Organization of Nanoparticles in Liquid Film. *Jpn. J. Appl. Phys.* (2004) **43:** 4434–4443.

[4] Bowden, N. Choi, I. S. Grzybowski, B. A. Whitesides, G. M. and Street, O. Mesoscale Self-Assembly of Hexagonal Plates Using Lateral Capillary Forces : Synthesis Using the ‘ Capillary Bond ’. *J. Am. Chem. Soc.* (1999) 5373–5391.

[5] Harris, C. J. Belcher, W. J. and Dastoor, P. C. Effect of film thickness and morphology on the performance of photoelectrochemical cells based on poly(terthiophene). *Sol. Energy Mater. Sol. Cells* (2007) **91:** 1127–1136.
[6] Krebs, F. C. Fabrication and processing of polymer solar cells: A review of printing and coating techniques. *Sol. Energy Mater. Sol. Cells* (2009) **93:** 394–412.
[7] Ulum, S. *et al.* Determining the structural motif of P3HT:PCBM nanoparticulate organic photovoltaic devices. *Sol. Energy Mater. Sol. Cells* (2013) **110:** 43–48.
[8] Paunov, V.N. Kralchevsky, P.A. Denkov, N.D. Ivanova, L.B. and Nagayamab, K. Capillary meniscus interaction between a microparticle and a wall. *Colloids and Surfaces*. (1992) **67:** 119–138.
[9] Dushkin, C.D. Yoshimura, H. and Nagayama, K. Direct Measurement of Nanonewton Capillary Forces. *J. Colloid Interface Sci.* (1996) **181:** 657–660.
[10] Leonardo, R.Di Saglimbeni, F. and Ruocco, G. Very-Long-Range Nature of Capillary Interactions in Liquid Films. *Physical Review Letters.* (2008) **100:** 106103,1–4.
[11] Allain, C. and Cloitre, M. Intersection between Particles Trapped at Fluid Interfaces I. Free-Energy Analysis of the Interaction between Two Horizontal Cylinders. *J. Colloid Interface Sci.* (1993) **157:** 269–277.
[12] Allain, C. and Cloitre, M. Intersection between Particles Trapped at Fluid Interfaces II. Exact and Asymptotic Solutions for the Force between Two Horizontal Cylinders. *J. Colloid Interface Sci.* (1993) **157:** 261–268.
[13] Fortes, M. A. Attraction and repulsion of floating particles. *Can. J . Chem.* (1982)
[14] Kralchevsky, P. A. and Nagayama, K. Capillary Forces between Colloidal Particles. *Langmuir* (1994) **10:** 23–36.
[15] Bragg, L. and Nye, J.F.A. Dynamical Model of a Crystal Structure. *Proc. R. Soc. London. Ser. A. Math. Phys. Sci.* (1947) **190:** 474 LP-481.
[16] Nicolson, M. The interaction between floating particles. *Math. Proc. Cambridge Philos. Soc.* (1949) **45:** 288–295.
[17] Gifford, W.A. and Scriven, L.E. On the attraction of floating particles. *Chem. Eng. Sci.* (1971) **26:** 287–297.
[18] Saif, T.A. On the capillary interaction between solid plates forming menisci on the surface of a liquid. *J. Fluid Mech.* (2002) **473:** 321–347.
[19] Yuan, J. and Cho, S.K. Cheerios Effect and its Control by Contact Angle Modulation. in *Advances in Contact Angle, Wettability and Adhesion* (ed. Mittal, K. L.) Wiley, (2015).
[20] Gautam, A. and Jameson, G.J. The capillary force between a bubble and a cubical particle. *Miner. Eng.* (2012) **36–38:** 291–299.
[21] Kralchevsky, P.A. and Nagayama, K. Capillary interactions between particles bound to interfaces , liquid films and biomembranes. *Advances in Colloid and Interface Science.* (2000) **85:** 145–192.
[22] Shinto, H. Komiyama, D. and Higashitani, K. Lateral Capillary Forces between Solid Bodies on Liquid Surface: A Lattice Boltzmann Study. *Langmuir.* (2006) **22:** 2058–2064.
[23] Shinto, H. Komiyama, D. and Higashitani, K. Lattice Boltzmann study of capillary forces between. *Adv. Powder Technol.* (2007) **18:** 643–662.
[24] Maenosono, S. Dushkin, C. D. Yamaguchi, Y. Nagayama, K. &andTsuji, Y. Effect of growth conditions on the structure of two-dimensional latex crystals: modeling. *Colloid Polym. Sci.* (1999) **277:** 1152–1161.
[25] Nishikawa, H. Maenosono, S. Yamaguchi, Y. and Okubo, T. Self-assembling process of colloidal particles into two-dimensional arrays induced by capillary immersion force: A simulation study with discrete element method. *J. Nanoparticle Res.* (2003) **5:**

103–110.
[26] Dushkin, C.D. Lazarov, G.S. Kotsev, S.N. Yoshimura, H. and Nagayama, K. Effect of growth conditions on the structure of two-dimensional latex crystals: Experiment. *Colloid Polym. Sci.* (1999) **277:** 914–930.
[27] Cundall, P.A. and Strack, O.D.L. A discrete numerical model for granular assemblies. *Geotechnique* (1979) **29:** 47–65.
[28] Pitois, O. and Chateau, X. Small Particle at a Fluid Interface: Effect of Contact Angle Hysteresis on Force and Work of Detachment. *Langmuir* (2002) **18:** 9751–9756.
[29] Kralchevsky, P.A. Paunov, V.N. Denkov, N.D. Ivanova, I.B. and Nagayama, K. Energetical and force approaches to the capillary interactions betweeen particles attatched to a liquid fluid interface. *J. Colloid Interface Sci.* (1993) **155:** 420–437.
[30] Heyes, D.M. and Branka, A.C. Brownian dynamic simulations of self-diffusion and shear viscosity of near-hard-sphere colloids. *Physical Review E.* (1994) **50:** 2377–2380.
[31] Hamaker, H.C. The London—van der Waals attraction between spherical particles. *Physica* (1937) **4:** 1058–1072.
[32] Fan, T.H. and Vinogradova, O.I. Hydrodynamic resistance of close-approached slip surfaces with a nanoasperity or an entrapped nanobubble. *Phys. Rev. E* (2005) **72:** 66306.
[33] Belhadj, M. Alper, H.E. and Levy, R.M. Molecular dynamics simulations of water with Ewald summation for the long range electrostatic interactions. *Chem. Phys. Lett.* (1991) **179:** 13–20.
[34] Putkaradze, V. Screening in particle attraction by capillary forces : from centimeter to nanometer scales. in *International Symposium on Nonlinear Theory and its Applications (NOLTA2005)* (2005). 573–576.
[35] Hansen, P.H.F. Rodner, S. and Bergstro, L. Structural Characterization of Dense Colloidal Films Using a Modified Pair Distribution Function and Delaunay Triangulation. *Langmuir* (2001) **17:** 4867–4875.